RSC Advances

PAPER

View Article Online
View Journal | View Issue

Cite this: *RSC Adv.*, 2015, **5**, 17216

Carbonized phenanthroline functionalized carbon as an alternative support: a strategy to intensify Pt activity and durability for methanol oxidation†

Wei Wang,*[ab] Yan Yang,[b] Fengxia Wang,[b] Wenkui Dong,[a] Xiaozhong Zhou[b] and Ziqiang Lei*[b]

Received 18th November 2014
Accepted 2nd February 2015

DOI: 10.1039/c4ra14790a

www.rsc.org/advances

In this study, a carbonized phenanthroline functionalized carbon support (CPF-C) has been prepared, which was used to load Pt nanoparticles to serve as an electrocatalyst for methanol oxidation. The results show that the performance of Pt in Pt/CPF-C is improved relative to that of industrially adopted Pt/C. The increase is mainly interpreted in terms of the synergistic effect between the stabilized Pt nanoparticles and nitrogen-functionalized CPF-C support. The novel CPF-C support presented here offers an alternative to the conventional carbon support to improve the performance of Pt applied in direct methanol fuel cells.

1. Introduction

Direct methanol fuel cells (DMFCs) have been considered as a promising alternative to conventional fossil fuels. Traditionally, Pt-based materials are thought of as the best electrocatalysts. However, as Pt has a high cost and its reserves are limited, extensive efforts have focused on promoting Pt performance by creating advanced novel catalysts. Approaches can be categorized into three types: firstly, formation of multi-component (Pt alloyed with other metals) or unique structures of Pt-based nanoparticles (core–shell, porous, sheet, *et al.*);[1–8] secondly, reducing the size of Pt-based nanoparticles;[9–15] lastly, using novel materials or alternative heteroatom carbon supports.[16–25] Undoubtedly, to move towards a genuinely practical DMFC technology, further improvements are still needed.[26]

For supports, such as carbon, carbon nanotube and graphene, the effect is to hinder agglomeration of loaded nanoparticles and to afford a high electron conductance between nanoparticles and the bulk electrode.[27] An advanced support can further affect the activity of the catalyst by an interaction between the support and nanoparticles. It can modify the electronic character of the nanoparticles, which would enhance the performance of the catalyst.[28]

It is reported that nitrogen-doping can enhance electron transfer properties.[29] The nitrogen-doping could not only change the physicochemical and electronic properties of the support, but also serve as basic or coordination sites to stabilize the small metal nanoparticles or activate some special substrates.[30] Thus, constructing nitrogen-functionalized carbon material has become one of the most attractive research topics because it is highly promising as alternative support for catalytic application.[31,32] Normally, nitrogen-functionalized carbon allotropes and their derivatives have been studied as alternative supports.[10,20,21,33–35] However, using phenanthroline as nitrogen source to synthesize nitrogen-functionalized alternative support for Pt in methanol oxidation is rarely reported.

Therefore, in this study, a catalyst of Pt nanoparticles on carbonized phenanthroline functionalized carbon support (CPF-C) has been prepared, characterized, and evaluated in the methanol oxidation reaction (MOR). The fabrication process results in uniformity in the particle size and strong particle-support interaction, benefiting for the performances of Pt/CPF-C catalyst. The catalyst exhibits high electrocatalytic properties, including high electrocatalytic activity, and relatively reliable stability and durability.

2. Experimental

2.1 CPF-C support synthesis

In a typical approach, phenanthroline (0.50 g), $NiCl_2 \cdot 6H_2O$ (0.24 g) and the pretreated carbon black (1.00 g, Vulcan XC-72R) were dissolved/dispersed in 40 ml ethanol and stirred for 12 h. Then, the ethanol was completely removed by a rotary evaporator. The remained solid was dried for 6 h at 80 °C and heat-treated at 800 °C for 2 h in tube furnace in N_2 atmosphere. Nextly, the solid was treated in 0.5 M H_2SO_4 for 12 h to remove

[a]*School of Chemical and Biological Engineering, Lanzhou Jiaotong University, Lanzhou 730070, China. E-mail: wangwchem@163.com; Fax: +86 931 4938755; Tel: +86 931 4938755*

[b]*Key Laboratory of Eco-Environment-Related Polymer Materials, Ministry of Education of China, Key Laboratory of Gansu Polymer Materials, College of Chemistry and Chemical Engineering, Northwest Normal University, Lanzhou 730070, China. E-mail: leizq@nwnu.edu.cn; leizq@hotmail.com; Fax: +86 931 7970261; Tel: +86 931 7970261*

† Electronic supplementary information (ESI) available. See DOI: 10.1039/c4ra14790a

unstable species, then centrifuged, filtrated and dried at 50 °C for 12 h. The product was named as CPF-C.

2.2 Pt/CPF-C catalyst synthesis

H_2PtCl_6 (66.4 mg) and sodium citrate (100.0 mg) were dissolved in 30 ml ethylene glycol (EG) and stirred for l h. The pH value was adjusted to ~8 by adding 5 wt% KOH/EG solution. Afterwards, the CPF-C powder (100.0 mg) was added with stirring and dispersing in an ultrasonic bath for 0.5 h, respectively. Then the suspension was heated at 180 °C for 4 h, centrifuged and washed with distilled water. The product was dried for 4 h at 50 °C. Finally, the Pt/CPF-C catalyst was obtained. For comparison, the industrially adopted commercial Pt/C was used as a reference (Johnson Matthey Company, 20 wt% metal loaded, HiSPEC 3000, 3.5 nm).

2.3 Characterization

Particle size and morphology were obtained on a transmission electron microscope (FEI TECNAI G^2 TF20 America). X-ray diffraction (XRD) patterns were recorded on a Rigaku D/Max-2400 (Japan) diffractometer, using Cu K_a radiation operated at 40 kV and 100 mA. X-ray photoelectron spectroscopy (XPS) (Thi-5702 America) was a monochromatic Al K_α X-ray source ($h\nu$ = 29.35 eV). The pyrolysis monitoring was performed on a thermogravimetric analysis (PerkinElmer, TG/DTA 6300, America).

The electrochemical experiments were performed on an electrochemical workstation (Autolab, PGSTAT128N, Eco Chemie, Netherlands). A glassy carbon (5 mm in diameter), a Pt wire and an Ag/AgCl were used as the working, the auxiliary and the reference electrodes, respectively. The working electrode was prepared as follows: 5 mg catalyst was dispersed ultrasonically in 1 ml Nafion/ethanol (0.25% Nafion). 8 μl suspensions were quantitatively transferred to the surface of polished glassy carbon electrode, followed by dried in air. Before each measurement, the solution was purged with high-purity N_2 for at least 10 min to ensure N_2 saturated.

3. Results and discussion

The CPF-C support was prepared from a phenanthroline chelate, which is easy to large-scale production. And the pyrolysis of phenanthroline chelate–carbon composite precursor was monitored by TG analysis shown in Fig. 1. The loss of adsorbed water is below 100 °C. The precursor begins to decompose at 170 °C and desorbs to volatile compounds between 170 and 450 °C. Then it is relatively stable between 450 and 680 °C. Finally, some of the phenanthroline chelate is decomposed and bounded, forming CPF-C as a nitrogen-functionalized graphite-like structure. The total weight loss is 73.5% of the initial weight at 800 °C. The structure and quality of CPF-C were also confirmed by Raman spectroscopy (see ESI Fig. S1†), and the results show that the CPF-C has a high graphitization degree compared to carbon. It would be related to the more defects and edge plane generated by the functionalized nitrogen onto the carbon surface. The resultant CPF-C can be an ideal catalytic support to homogeneously immobilize and stabilize small Pt nanoparticles, and would demonstrate high catalytic activity and durability in MOR.

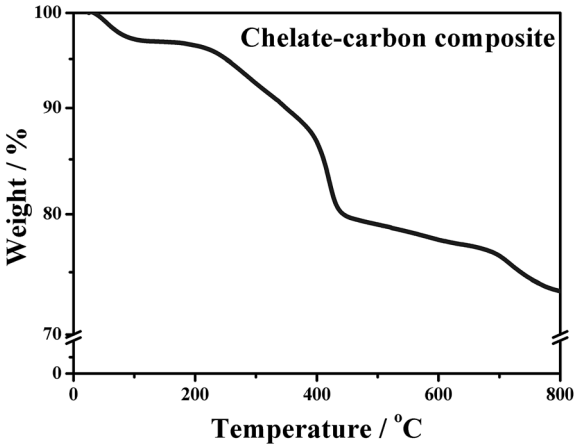

Fig. 1 TG spectrum of preparing CPF-C support from the precursor of phenanthroline chelate–carbon composite.

The morphology of as-prepared Pt/CPF-C catalyst is shown in Fig. 2a. The small Pt nanoparticles are formed by anchoring the Pt ion on the CPF-C surface and subsequently reducing to the fine particles, without any significant agglomeration. Based on two hundred Pt particles randomly selected, Fig. 2b shows the corresponded particle size distribution histograms. The particles are dispersed on the support with narrow size distribution and the mean size of the Pt particles is about 3.9 nm. The Pt/CPF-C particles are slightly larger than that of commercial Pt/C (3.5 nm). However, based on the synergistic effect between the Pt nanoparticles and CPF-C support, the Pt/CPF-C also shows the high performance in MOR below. The high-magnification transmission electron microscope (TEM) image of an individual Pt nanoparticle of Pt/CPF-C shows its crystalline structure in Fig. 2c. The measured interplanar spacing of the lattice fringes is 0.23 nm, which is the lattice spacing of the (111) plane in face-centered cubic (*fcc*) Pt.[10,36] As shown in Fig. 2d, the selected area electron diffraction (SAED) on Pt/CPF-C catalyst shows concentric rings composed of bright discrete diffraction spots that can be indexed to Pt (*fcc*), indicating the polycrystalline of the Pt nanoparticles.

The XPS measurements were performed to probe the chemical composition of the Pt/CPF-C catalyst. As shown in Fig. 3a, the XPS spectrum of Pt/CPF-C catalyst shows the presence of N 1s, C 1s, O 1s and Pt 4f peaks clearly without any other signals. The N 1s XPS results for the as-prepared Pt/CPF-C catalyst shown in Fig. 3b, and it is deconvoluted using three different binding energies: pyridinic-nitrogen (398.4 eV, 15.1%), pyrrolic-nitrogen (400.0 eV, 48.1%) and graphitic-nitrogen (401.7 eV, 36.8%). Obviously, the pyrrolic-nitrogen is dominant component. As shown in Fig. 3c, the Pt 4f XPS spectra contain two peaks corresponding to Pt $4f_{7/2}$ and $4f_{5/2}$ states from the spin–orbital splitting. The peaks at 71.9 eV (Pt $4f_{7/2}$) and 75.2 eV (Pt $4f_{5/2}$) are attributed to Pt^{2+} specie, while 70.9 eV (Pt $4f_{7/2}$) and 74.2 eV (Pt $4f_{5/2}$) are accorded to Pt^0 specie.[37] It is known that the nitrogen species can form a strong interaction with Pt.[38]

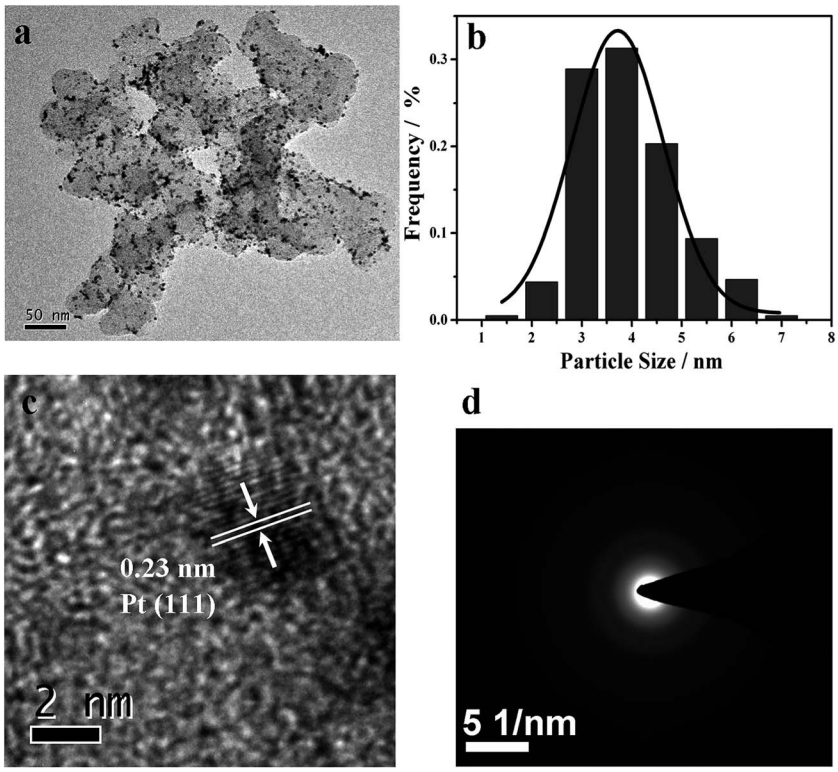

Fig. 2 The morphology of Pt/CPF-C catalyst: (a) low-magnification TEM image; (b) size distribution histograms; (c) high-magnification TEM image; (d) corresponded SAED pattern.

XRD measurements were performed to investigate the crystal structures of the Pt/CPF-C and Pt/C catalysts. From the Fig. 3d, the first broad peaks are attributed to the graphite structure of (200) plane. Other remaining peaks are assigned to the (111), (200), (220) and (311) crystal facets of Pt (*fcc*) crystal structure. Using the Debye–Scherrer equation relating to the (111) peak broadness, the mean particle size could be evaluated from the literature.[39] The average particle size of the Pt/C and Pt/CPF-C is 3.6 nm and 3.8 nm, respectively. These results are consistent with the results obtained from TEM. It is worth to note that, the C (200) peak of Pt/CPF-C shifts to lower 2θ value compared to that of Pt/C (inserted in Fig. 3d). Additionally, the peak intensity is relatively decreased. These indirectly prove that carbon has been functionalized by carbonized phenanthroline precursor.

To demonstrate the advantage of CPF-C support, the electrochemical performance of Pt/CPF-C was compared with Pt/C. The cyclic voltammogram (CV) curves show the general features of Pt. As shown in Fig. 4a, the well-defined hydrogen adsorption/desorption peaks and characteristic peaks for the redox process of Pt are observed on Pt/CPF-C and Pt/C catalysts. The electrochemically active surface area (ECSA) of catalysts was evaluated by the hydrogen adsorption/desorption of Pt according to literature.[40] The Pt/CPF-C shows a larger ECSA value (86.3 $m^2\ g^{-1}{}_{Pt}$) than that of the Pt/C (45.7 $m^2\ g^{-1}{}_{Pt}$). The nitrogen-functionalized structure of CPF-C support can modify nucleation and growth kinetics during the deposition of Pt nanoparticles, which results in high dispersion, makes the support surface chemically active for the enhanced interaction between Pt and CPF-C. Therefore, these, as well as probably a better conductivity of the CPF-C support, substantially may lead to a large ECSA value for Pt/CPF-C catalyst.[41,42]

MOR measurements were further performed in 0.5 M H_2SO_4 and 0.5 M CH_3OH solution in Fig. 4b. The MOR peaks (about 0.7 V *vs.* Ag/AgCl) are observed in the forward scan and anodic peaks (about 0.5 V *vs.* Ag/AgCl) are detected during the reverse scan. The mass activity of the Pt/CPF-C catalyst is 0.443 A $mg^{-1}{}_{Pt}$, which is about two times higher than that of the Pt/C (0.207 A $mg^{-1}{}_{Pt}$). These are consistent with the ECSA analysis. The ratio, the forward-scan peak current (I_f) *versus* the reverse-scan peak current (I_b), is a key index for evaluating the catalyst's tolerance to the accumulation of intermediate carbonaceous species.[38] A high I_f/I_b indicates a good poisoning tolerance of the catalyst for MOR. The I_f/I_b ratio of Pt/CPF-C is 0.86, which is higher than that of Pt/C (0.78). It implies the Pt/CPF-C has a better tolerance to CO and more complete oxidation of methanol to CO_2 than that of the Pt/C catalyst. Furthermore, from window inserted in Fig. 4b, the onset potential for the Pt/CPF-C catalyst is lower than that of Pt/C. This change indicates that the Pt/CPF-C catalyst could catalyze MOR at low potential, demonstrating that the Pt/CPF-C has desirable kinetics for MOR.

Long-term stability and durability of catalyst are critical requirement for electrochemical energy device applications. MOR cycling and chronoamperometry (CA) were carried out to examine the stability and durability of the Pt/CPF-C and Pt/C catalysts. As can be seen in Fig. 4c, based on Pt mass, the Pt/CPF-C catalyst loses 58.8% of MOR activity after 500 cycles,

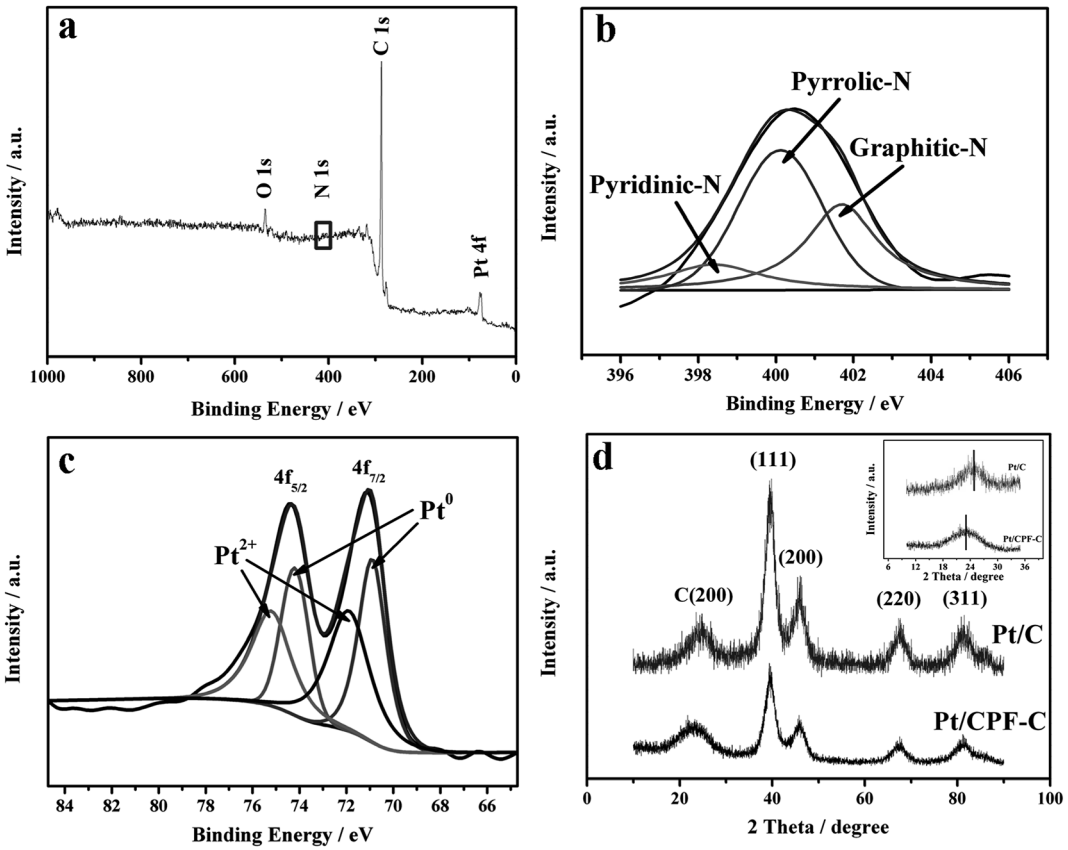

Fig. 3 XPS spectrum of Pt/CPF-C (a); N 1s XPS spectrum of Pt/CPF-C (b); Pt 4f XPS spectrum of Pt/CPF-C (c); XRD patterns of Pt/CPF-C and Pt/C (d). Insert: enlarged C (200) peaks.

whereas that of the Pt/C catalyst has decreased by 64.0%. During the electrocatalytic processes, the increased Pt particle size, the aggregation of Pt particles, and the falling off of Pt particles from the support are considered to be the major reasons for the Pt MOR activity loss.[43] Obviously, the rate of the degradation of the Pt/CPF-C catalyst is relatively slower than that of the Pt/C catalyst. This is considered that the nitrogen-functionalized support in Pt/CPF-C catalyst makes the Pt particles less vulnerable to dissolute and aggregate than those supported on the carbon, leading to a better stability for MOR.

Although the complete oxidation of methanol yields CO_2 as the final product, the complete oxidation seldom takes place. There are numerous intermediate products, including adsorbed poisons, formed during MOR. Therefore, the decay of current implies the poisoning of the catalyst. CA measurements of Pt/CPF-C and Pt/C were performed at 0.6 V (*vs.* Ag/AgCl) for 3000 s. As shown in Fig. 4d, the initial current density for Pt/CPF-C is greater than that of the Pt/C, implying a greater number of active sites available per unit of surface area. Obviously, the Pt/CPF-C has a higher current density than that of Pt/C over the whole process, showing that it has a higher poison-tolerance. The linear decay of the current at times greater than 500 s may be characterised by the long-term poisoning rate (δ) as follows:[44]

$$\delta = (100/I_0) \times (\mathrm{d}I/\mathrm{d}t)_{t>500\ \mathrm{s}}\ (\%\ \mathrm{s}^{-1})$$

where I_0 is the current at the start of polarisation back extrapolated from the linear current decay, $(\mathrm{d}I/\mathrm{d}t)_{t>500\ \mathrm{s}}$ is the slope of the linear portion of the current decay. The calculated δ values of Pt/CPF-C and Pt/C are 0.021 and 0.288, respectively. Clearly, the strong interaction between Pt nanoparticles and CPF-C substrate leads to relatively improved stability and durability of the Pt/CPF-C catalyst. These are also consistent with MOR cycling tests in Fig. 4c.

Fig. 5a shows a typical linear sweep voltammogram (LSV) at the scan rate of 1 mV s^{-1} in 0.5 M H_2SO_4 + 0.5 M CH_3OH solution, which is close to a steady-state polarization curve of MOR.[45] Obviously, the current of the Pt/CPF-C catalyst remains higher in contrast with the Pt/C catalyst throughout the test, which is similar to the results of Fig. 4b above. The corresponded Tafel plots of the MOR are shown in Fig. 5b, calculated from the quasi-steady-state curves in Fig. 5a. It shows two linear regions with the respective Tafel slope. The Tafel slope of the Pt/CPF-C is 116.3 mV dec^{-1} (<−0.45 V *vs.* Ag/AgCl), and it turns into 194.4 mV dec^{-1} (>−0.45 V *vs.* Ag/AgCl). While, Pt/C is 111.8 mV dec^{-1} (<−0.42 V *vs.* Ag/AgCl), and it turns into 238.9 mV dec^{-1} (>−0.42 V *vs.* Ag/AgCl). As the potential increasing, two Tafel slopes from low values increases up to high values. It indicates the possible changes of rate-determining step and mechanism within a given potential range. It has been reported that the splitting of the first C–H bond of methanol molecules

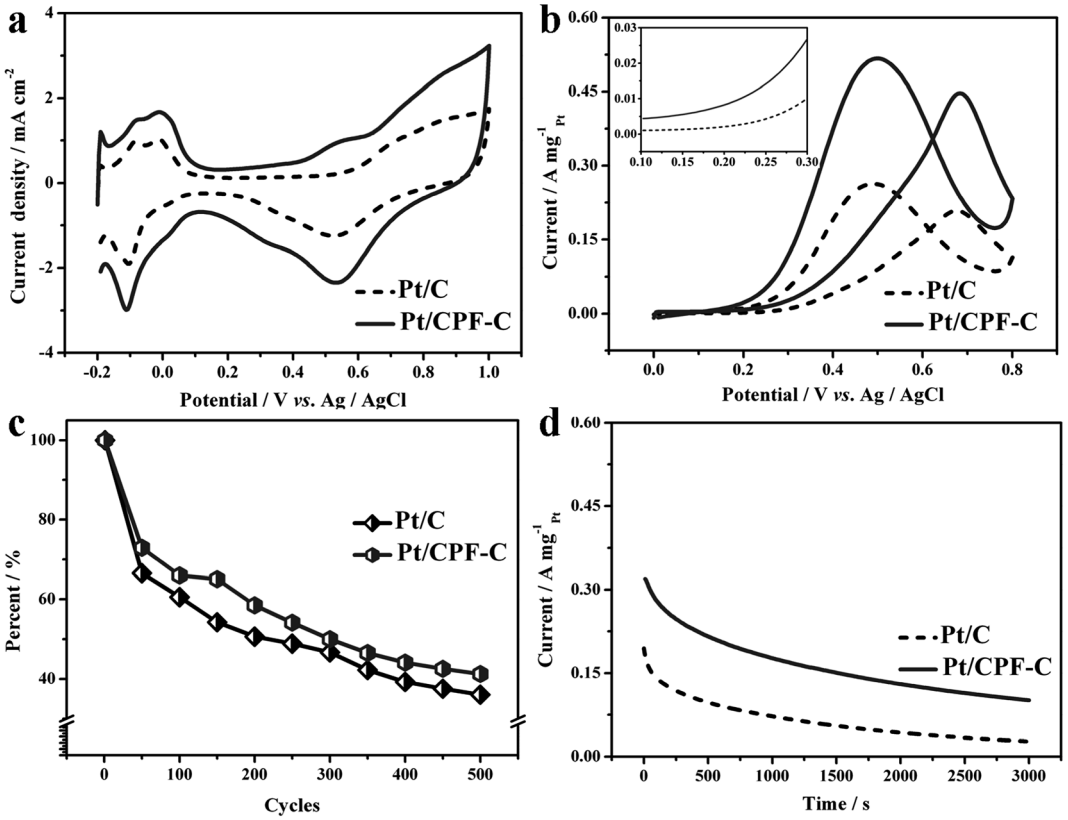

Fig. 4 CV of Pt/CPF-C and Pt/C in 0.5 M H_2SO_4 solution. Scan rate: 50 mV s^{-1} (a); MOR of Pt/CPF-C and Pt/C in 0.5 M H_2SO_4 + 0.5 M CH_3OH solution. Scan rate: 50 mV s^{-1} (b). Inserted: enlarged window from 0.1 V–0.3 V; decreases of peak currents of Pt/CPF-C and Pt/C on cycling in 0.5 M H_2SO_4 + 0.5 M CH_3OH (c); CA of Pt/CPF-C and Pt/C in 0.5 M H_2SO_4 + 0.5 M CH_3OH (d). Inserted: current after 3000 s; fixed potential: 0.6 V.

and mass transfer of methanol are the rate-determining step at relatively low and high potentials, respectively.[46,47]

The effect of temperature on MOR was also investigated. Fig. 6a and c show the MOR on the Pt/CPF-C and Pt/C catalysts at different temperature values, respectively. Obviously, current density for MOR increases with the temperatures rising. Additionally, the MOR current obtained in the forward sweep (about 0.65 V *vs.* Ag/AgCl) is raised by a factor of 6 as the temperature increasing from 278 to 308 K, while the negative sweeps display vertical increase of the reverse oxidation peaks (about 0.5 V *vs.* Ag/AgCl), which are more prominent at higher temperatures. Similar to the literature,[48] these indicate the residues remaining unoxidized on the surface of catalyst during the forward sweep can only be oxidized at higher potentials.

The comparison of activation energy values can give insight into the performance difference between two catalysts in MOR. The value of the activation energy can be obtained from the slope of the linear relationship between log j and $1/T$. As can be

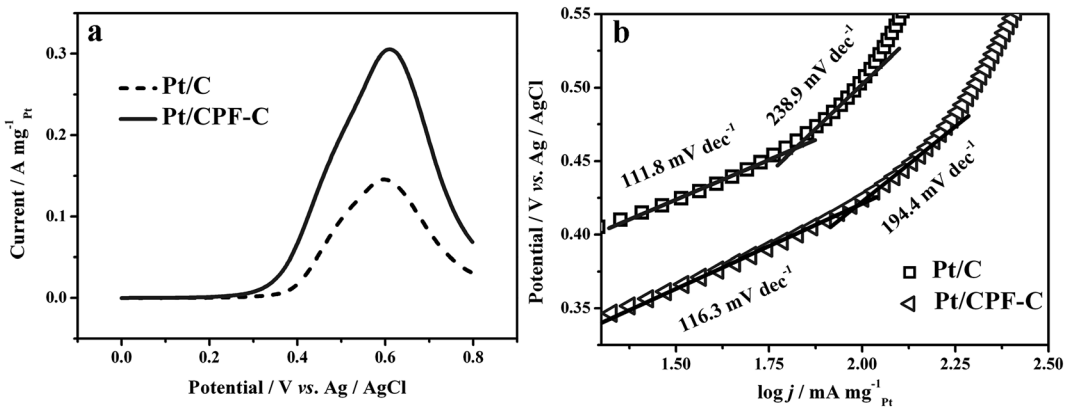

Fig. 5 LSV of Pt/CPF-C and Pt/C in 0.5 M H_2SO_4 + 0.5 M CH_3OH solution. Scan rate: 1 mV s^{-1} (a); the corresponded Tafel plots of Pt/CPF-C and Pt/C (b).

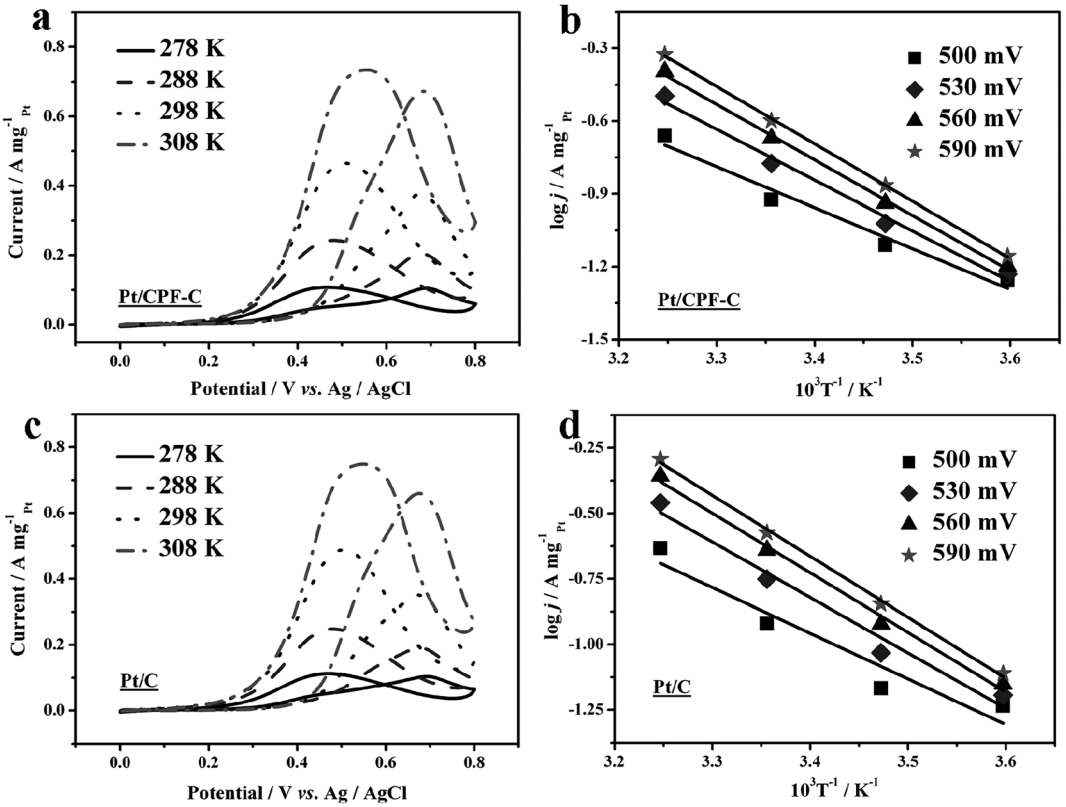

Fig. 6 MOR tests on different temperatures for Pt/CPF-C (a) and Pt/C (c) in 0.5 M H_2SO_4 + 0.5 M CH_3OH solution. Scan rate: 50 mV s^{-1}; the corresponded Arrhenius plots of Pt/CPF-C (b) and Pt/C (d).

seen in Fig. 6b and d, well-linear relation between log j and $1/T$ is obtained in the temperature range from 278 to 308 K. And the average apparent activation energy has been determined. The lower activation energy value of 17.51 kJ mol^{-1} on Pt/CPF-C for MOR is obtained against 17.61 kJ mol^{-1} on Pt/C. A slight low activation energy also means high intrinsic activity and fast charge-transfer process. In other words, any reduction in the activation energy would be translated into the high intrinsic activity. It is reasonable to deduce that nitrogen-functionalized CPF-C support is beneficial for Pt/CPF-C catalyst towards MOR in DMFCs.

4. Conclusion

In this study, a carbonized phenanthroline functionalized carbon support (CPF-C) has been prepared to load Pt nanoparticles towards MOR. Compared to commercial Pt/C catalyst, the as-synthesized Pt/CPF-C catalyst shows relatively high performance, with respect to onset potential, mass activity, stability and durability. The temperature investigation also shows that the Pt/CPF-C catalyst has a relatively low activation energy value for MOR. Consequently, the CPF-C can be used as a promising alternative support to intensify Pt applied in DMFCs.

Acknowledgements

We thank to the National Natural Science Foundation of China (no. 21174114), the program for Changjiang Scholars and Innovative Research Team in University (IRT1177), Key Laboratory of Eco-Environment-Related Polymer Materials of Ministry of Education and Key Laboratory of Polymer Materials of Gansu Province.

References

1 S. Guo, S. Zhang, D. Su and S. Sun, *J. Am. Chem. Soc.*, 2013, **135**, 13879.
2 P. Malacrida, M. Escudero-Escribano, A. Verdaguer-Casadevall, I. E. L. Stephens and I. Chorkendorff, *J. Mater. Chem. A*, 2014, **2**, 4234.
3 L. Wang and Y. Yamauchi, *J. Am. Chem. Soc.*, 2013, **135**, 16762.
4 S. I. Choi, S. Xie, M. Shao, J. H. Odell, N. Lu, H. C. Peng, L. Protsailo, S. Guerrero, J. Park, X. Xia, J. Wang, M. J. Kim and Y. Xia, *Nano Lett.*, 2013, **13**, 3420.
5 S. Xie, S. I. Choi, N. Lu, L. T. Roling, J. A. Herron, L. Zhang, J. Park, J. Wang, M. J. Kim, Z. Xie, M. Mavrikakis and Y. Xia, *Nano Lett.*, 2014, **14**, 3570.
6 E. Antolini, *Mater. Chem. Phys.*, 2003, **78**, 563.
7 S. Mukerjee and R. C. Urian, *Electrochim. Acta*, 2002, **47**, 3219.
8 X. Zhao, M. Yin, L. Ma, L. Liang, C. Liu, J. Liao, T. Lu and W. Xing, *Energy Environ. Sci.*, 2011, **4**, 2736.
9 Y. Takasu, H. Itaya, T. Iwazaki, R. Miyoshi, T. Ohnuma, W. Sugimoto and Y. Murakami, *Chem. Commun.*, 2001, 341.

10 Z. Sun, Y. Zhao, Y. Xie, R. Tao, H. Zhang, C. Huang and Z. Liu, *Green Chem.*, 2010, **12**, 1007.
11 B. Sheng, L. Hu, T. Yu, X. Cao and H. Gu, *RSC Adv.*, 2012, **2**, 5520.
12 C. Nethravathi, E. A. Anumol, M. Rajamathi and N. Ravishankar, *Nanoscale*, 2011, **3**, 569.
13 Y. Mu, H. Liang, J. Hu, L. Jiang and L. Wan, *J. Phys. Chem. B*, 2005, **109**, 22212.
14 Y. Li, W. Gao, L. Ci, C. Wang and P. M. Ajayan, *Carbon*, 2010, **48**, 1124.
15 W. X. Chen, J. Y. Lee and Z. Liu, *Chem. Commun.*, 2002, 2588.
16 Y. C. Kimmel, X. Xu, W. Yu, X. Yang and J. G. Chen, *ACS Catal.*, 2014, **4**, 1558.
17 M. Roca-Ayats, G. García, J. L. Galante, M. A. Peña and M. V. Martínez-Huerta, *J. Phys. Chem. C*, 2013, **117**, 20769.
18 G. Agostini, C. Lamberti, R. Pellegrini, G. Leofanti, F. Giannici, A. Longo and E. Groppo, *ACS Catal.*, 2014, **4**, 187.
19 K. An, S. Alayoglu, N. Musselwhite, S. Plamthottam, G. Melaet, A. E. Lindeman and G. A. Somorjai, *J. Am. Chem. Soc.*, 2013, **135**, 16689.
20 C. Alegre, M. Gálvez, R. Moliner, V. Baglio, A. Aricò and M. Lázaro, *Appl. Catal., B*, 2014, **147**, 947.
21 J. Liang, Y. Jiao, M. Jaroniec and S. Z. Qiao, *Angew. Chem., Int. Ed.*, 2012, **51**, 11496.
22 D. Higgins, M. A. Hoque, M. H. Seo, R. Wang, F. Hassan, J. Y. Choi, M. Pritzker, A. Yu, J. Zhang and Z. Chen, *Adv. Funct. Mater.*, 2014, **24**, 4325.
23 Z. Liu, J. Y. Lee, W. Chen, M. Han and L. M. Gan, *Langmuir*, 2004, **20**, 181.
24 M. Carmo, V. A. Paganin, J. M. Rosolen and E. R. Gonzalez, *J. Power Sources*, 2005, **142**, 169.
25 G. Hu, F. Nitze, H. R. Barzegar, T. Sharifi, A. Mikołajczuk, C. W. Tai, A. Borodzinski and T. Wågberg, *J. Power Sources*, 2012, **209**, 236.
26 M. K. Debe, *Nature*, 2012, **486**, 43.
27 E. Gracia-Espino, X. Jia and T. Wågberg, *J. Phys. Chem. C*, 2014, **118**, 2804.
28 N. I. Kim, J. Y. Cheon, J. H. Kim, J. Seong, J. Y. Park, S. H. Joo and K. Kwon, *Carbon*, 2014, **72**, 354.
29 D. W. Wang, I. R. Gentle and G. Q. Lu, *Electrochem. Commun.*, 2010, **12**, 1423.
30 Z. Li, J. Liu, C. Xia and F. Li, *ACS Catal.*, 2013, **3**, 2440.
31 D. Liu, L. Yang, J. S. Huang, Q. H. Guo and T. Y. You, *RSC Adv.*, 2014, **4**, 13733.
32 J. N. Tiwari, K. C. Kemp, K. Nath, R. N. Tiwari, H. G. Nam and K. S. Kim, *ACS Nano*, 2013, **7**, 9223.
33 T. Zhou, H. Wang, J. Key, S. Ji, V. Linkov and R. Wang, *RSC Adv.*, 2013, **3**, 16949.
34 J. Cao, Y. Chu and X. Tan, *Mater. Chem. Phys.*, 2014, **144**, 17.
35 Z. Liu, F. Su, X. Zhang and S. W. Tay, *ACS Appl. Mater. Interfaces*, 2011, **3**, 3824.
36 Y. Wei, Z. Zhao, J. Liu, C. Xu, G. Jiang and A. Duan, *Small*, 2013, **9**, 3957.
37 H. H. Li, S. Zhao, M. Gong, C. H. Cui, D. He, H. W. Liang, L. Wu and S. H. Yu, *Angew. Chem., Int. Ed.*, 2013, **52**, 7472.
38 H. Huang, S. Yang, R. Vajtai, X. Wang and P. M. Ajayan, *Adv. Mater.*, 2014, **26**, 5160.
39 V. I. Zaikovskii, K. S. Nagabhushana, V. V. Kriventsov, K. N. Loponov, S. V. Cherepanova, R. I. Kvon, H. Bönnemann, D. I. Kochubey and E. R. Savinova, *J. Phys. Chem. B*, 2006, **110**, 6881.
40 J. Zhao, H. Yu, Z. Liu, M. Ji, L. Zhang and G. Sun, *J. Phys. Chem. C*, 2014, **118**, 1182.
41 G. Hu, F. Nitze, T. Sharifi, H. R. Barzegar and T. Wagberg, *J. Mater. Chem.*, 2012, **22**, 8541.
42 Y. W. Lee, M. Kim and S. W. Han, *Chem. Commun.*, 2010, **46**, 1535.
43 C. Zhang, L. Xu, N. Shan, T. Sun, J. Chen and Y. Yan, *ACS Catal.*, 2014, **4**, 1926.
44 J. Jiang and A. Kucernak, *J. Electroanal. Chem.*, 2003, **543**, 187.
45 S. Cavaliere, S. Subianto, I. Savych, M. Tillard, D. J. Jones and J. Rozière, *J. Phys. Chem. C*, 2013, **117**, 18298.
46 G. Wu, L. Li and B. Q. Xu, *Electrochim. Acta*, 2004, **50**, 1.
47 H. Wang, R. Wang, H. Li, Q. Wang, J. Kang and Z. Lei, *Int. J. Hydrogen Energy*, 2011, **36**, 839.
48 S. S. Mahapatra, A. Dutta and J. Datta, *Electrochim. Acta*, 2010, **55**, 9097.

